Journal of Comparative Neurology

WILEY

JCN RESEARCH IN SYSTEMS NEUROSCIENCE THE JOURNAL OF COMPARATIVE NEUROLOGY

RESEARCH ARTICLE OPEN ACCESS

Dopaminergic Innervation of the Nidopallium Caudolaterale in the Japanese Quail

Defne Albayrak[1] | Sinem Gencturk[1] | Kevin B. Haselhuhn[2] | Cem Sevinc[1] | Onur Güntürkün[2] | Mehdi Behroozi[2] | Noemi Rook[2] | Gunes Unal[1]

[1]Behavioral Neuroscience Laboratory, Department of Psychology, Boğaziçi University, Istanbul, Turkey | [2]Department of Biopsychology, Institute of Cognitive Neuroscience, Faculty of Psychology, Ruhr University, Bochum, Germany

Correspondence: Noemi Rook (noemi.rook@ruhr-uni-bochum.de) | Gunes Unal (gunes.unal@bogazici.edu.tr)

Received: 18 October 2025 | **Revised:** 9 March 2026 | **Accepted:** 18 March 2026

Keywords: convergent evolution | dopamine | fiber density | Japanese quail | nidopallium caudolaterale | pallium | prefrontal cortex

ABSTRACT

Convergent evolution illustrates how distantly related lineages develop comparable traits and abilities in response to similar ecological pressures. In birds, the nidopallium caudolaterale (NCL) is an executive function hub analogous to the mammalian prefrontal cortex, despite their distant roots and major differences in gross structure. While the NCL has been studied in pigeons, songbirds, and chickens, its organization in other Galliformes remains unclear. Here, we investigated the NCL in the Japanese quail (*Coturnix japonica*), a Galliform species commonly used in studies of reproductive behavior and appetitive conditioning. Using immunohistochemistry for tyrosine hydroxylase, we mapped dopaminergic projections from the ventral tegmental area and substantia nigra, quantified fiber density relative to surrounding pallial regions, and characterized axonal arborizations. We identified postsynaptic targets of tyrosine hydroxylase-positive fibers and examined their neurochemical profiles, including putative glutamatergic neurons expressing CaMKIIa and interneuron subpopulations expressing parvalbumin, calbindin, calretinin, or secretagogin. The NCL of the Japanese quail exhibited dense dopaminergic innervation primarily targeting principal neurons, with only sparse *en passant* contacts on interneuron populations, following the pattern observed in other Galliformes. These findings indicate that dopaminergic modulation of the NCL is conserved across Galliformes and support the use of the Japanese quail as a model for studying executive circuits and cognitive neurobiology in birds.

1 | Introduction

Convergent evolution demonstrates that similar selective pressures can independently shape analogous morphological, physiological, or behavioral traits in phylogenetically distant lineages, highlighting the existence of constrained evolutionary solutions to common ecological challenges (Bolnick et al. 2018; Güntürkün 2005a). This process underlies the emergence of advanced cognitive abilities in birds, which in some cases rival those of mammals (Güntürkün 2005a, 2012; Pika et al. 2020; Seed et al. 2009). Although birds and mammals last shared a common ancestor over 300 million years ago (Benton and Donoghue 2007), both lineages independently evolved brain regions associated with executive functions: the nidopallium caudolaterale (NCL) in birds and the prefrontal cortex (PFC) in mammals (Güntürkün 2005a, 2005b, 2012; Seed et al. 2009). In this study, we characterized the primary neuromodulatory pathway—dopaminergic innervation—in the NCL of the Japanese quail (*Coturnix japonica*), a member of the Phasianidae family that serves as a valuable model for studying reproductive biology (Ball and Balthazart

Defne Albayrak and Sinem Gencturk contributed equally to this study.

2010; Ottinger et al. 1997) and appetitive conditioning (Akins et al. 1994; Domjan et al. 1986, 1988; Gutiérrez and Domjan 1997). We delineated the origins of the dopaminergic projections to the NCL, characterized their neurochemical composition, described their axonal arborization within target structures, and identified specific postsynaptic targets.

At first glance, the comparison between PFC and NCL appears counterintuitive. The mammalian PFC is embedded in a six-layered neocortex in the anterior of the telencephalon, while the NCL, as part of the avian pallium, exhibits a nuclear rather than laminar organization and is located in the most caudal part of the forebrain. In addition, the avian pallium lacks pyramidal neurons, a hallmark cell type of mammalian neocortex (Nomura et al. 2008). However, a growing body of evidence demonstrates that these differences in gross anatomy and topography mask profound similarities in connectivity, neurochemistry, and function (Güntürkün 2005a, 2005b, 2012; Güntürkün et al. 2021; Güntürkün and Bugnyar 2016). Both PFC and NCL integrate multimodal sensory inputs, maintain reciprocal connections with motor and limbic structures, and receive dense dopaminergic innervation from the ventral tegmental area (VTA) and substantia nigra (SN). Dopamine, in turn, modulates neuronal excitability and synaptic plasticity in these regions, supporting core executive operations such as working memory, attentional control, and decision-making (Durstewitz et al. 1999; Seamans and Yang 2004; Ott and Nieder 2019). Ablation studies have demonstrated that disrupting the NCL impairs performance in delayed alternation tasks (Mogensen and Divac 1982, 1993), hinders reversal learning and cognitive flexibility (Hartmann and Güntürkün 1998; Lissek et al. 2002), and compromises complex decision-making (Kalenscher et al. 2003), resembling the effects of PFC lesions in mammals. These parallels underscore the notion that PFC and NCL represent convergent solutions to the challenge of implementing flexible cognition in two distantly related vertebrate lineages.

The NCL was first identified in pigeons through behavioral and biochemical evidence, and its boundaries have been objectively delineated using quantitative receptor autoradiography (Divac et al. 1985; Herold et al. 2011; Mogensen and Divac 1982). Given the diversity of the mammalian PFC and the variation in cognitive abilities across bird species, subsequent research has aimed to characterize the fundamental features of the NCL across different avian taxa and to investigate its interspecific variability (Güntürkün et al. 2021; von Eugen et al. 2020). To date, the NCL has been described and studied not only in pigeons but also in zebra finches (*Taeniopygia guttata*), carrion crows (*Corvus corone*), chickens (*Gallus gallus domesticus*), and Eurasian blackcaps (*Sylvia atricapilla*; Kobylkov et al. 2022; von Eugen et al. 2020). Even in Nile crocodiles, which diverged evolutionarily before birds (Shine 2013), a primitive NCL-like region has been proposed within the dorsal ventricular ridge. This area exhibits comparatively dense tyrosine hydroxylase (TH) immunopositive (+) labeling and, in some locations, TH+ basket-like formations (Billings et al. 2020).

Galliformes occupy an especially important position in this comparative framework. As one of the most ancient avian lineages (Prum et al. 2015), they provide insight into the ancestral state of pallial organization. The chicken has been the primary galliform model, with its NCL well characterized in terms of boundaries, dopaminergic innervation, and connectivity (von Eugen et al. 2020; Puelles et al. 2018). In addition to the core NCL, chickens possess an accessory dopaminergic cluster, the nidopallium caudolaterale island fields (NCIF), raising the question of whether this feature is a general galliform trait or a chicken-specific specialization. Comparative studies across other galliform species are essential to address this issue, and the Japanese quail offers a particularly valuable model. Although phylogenetically close to the chicken, quail differ markedly in ecology, behavior, and life history: While chickens are domesticated, flock-living foragers, quail are ground-dwelling, migratory birds with short-range flight and distinct reproductive strategies. They also vary in social structure, mating systems, and vocal repertoires. Moreover, quails are widely used in laboratory research across neuroendocrinology and learning paradigms (Akins et al. 1994; Ball and Balthazart 2010; Domjan et al. 1986, 1988; Ottinger et al. 1997; Gutiérrez and Domjan 1997). If the quail NCL closely resembles that of chickens, it would suggest that dopaminergic executive circuits are deeply conserved across Galliformes; conversely, structural or neurochemical differences could indicate adaptive modifications shaped by species-specific ecological pressures.

In addition to delineating the boundaries of the NCL, it is critical to understand the cellular targets of dopaminergic input. In mammals, dopamine modulates both excitatory pyramidal neurons and inhibitory interneurons, balancing persistent activity with dynamic flexibility (Durstewitz and Seamans 2002; Seamans and Yang 2004). Whether similar mechanisms exist in the avian NCL remains an open question. Pallial cell types in avian species are developmentally conserved across amniotes, with glutamatergic and GABAergic neurons constituting the major groups (Colquitt 2022; Spool et al. 2021; Zaremba et al. 2025). Glutamatergic neurons are distinguished from GABAergic cells by their electrophysiological properties, neurochemistry, and morphology. They serve as the principal excitatory projection cells in songbird pallial regions and are characterized by the expression of calcium/calmodulin-dependent protein kinase II alpha (CaMKIIa), similar to mammalian pallium (Lee et al. 2012; Spool et al. 2021). GABAergic neurons, by contrast, make up similar proportions as in the mammalian pallium (approximately 10%–20% of pallial neurons), exhibit comparable electrophysiological properties, and share developmental origins from different ganglionic eminences (Spool et al. 2021; Zaremba et al. 2025). Despite these similarities in proportion and origin, avian species exhibit fewer GABAergic subclasses, compared to mammals (Zaremba et al. 2025).

GABAergic interneuron types are conventionally classified based on calcium-binding protein (CaBP) expressions as in mammals. The most extensively studied CaBP in the avian pallium is parvalbumin (PV; Kuenzel et al. 2011; Pinaud and Mello 2007). PV+ cells in songbird pallial areas are GABAergic and display firing properties analogous to mammalian cortical PV+ neurons (Spool et al. 2021). Other major CaBP classes, calbindin (CB) and calretinin (CR), are less extensively studied in avian brains. These proteins are predominantly GABAergic in mammals and have been used to characterize GABAergic cells in songbird pallial regions (Pinaud and Mello 2007; Zhao et al. 2013). Traditional markers such as GAD, the enzyme converting glutamate to GABA, have often failed to identify GABAergic postsynaptic

targets of TH+ baskets in pigeons (Durstewitz et al. 1998), and GAD or GABA immunostaining is highly variable in both birds and mammals (McCasland and Hibbard 1997; Pinaud and Mello 2007), highlighting the need for CaBP-based characterization. In zebra finches, TH+ baskets in the NCL originating from the SN and VTA are GABAergic and can be defined by the spatial distribution of PV, CB, CR, and secretagogin (SCGN; Mitra et al. 2022). However, no comparable evidence exists for galliform species, which differ from songbirds in dopaminergic organization and neuronal counts (Kocourek et al. 2025; Kubikova et al. 2010).

Taken together, these considerations underscore the value of the Japanese quail for studying avian executive circuits. As a close relative of the chicken, quail allow us to test whether the dopaminergic organization of the NCL is a conserved feature of Galliformes or exhibits flexibility in response to ecological and behavioral differences. Here, we mapped the quail NCL based on dopaminergic innervation, quantified fiber density relative to surrounding pallial regions, and characterized both the postsynaptic targets and neurochemical profile of VTA/SN-derived dopaminergic inputs.

2 | Methods

2.1 | Specimen

This study used brain tissue from 15 adult Japanese quails (*Coturnix japonica*) obtained from local breeders in Istanbul. All procedures were approved by the Boğaziçi University Ethics Committee for the Use of Animals in Experiments (Approval No: 2023-15), adhered to the German Animal Welfare Law for the prevention of cruelty to animals, and complied with Directive 2010/63/EU of the European Parliament and of the Council of September 22, 2010.

2.2 | Dissection

The animals were euthanized with an overdose of pentobarbital and perfused transcardially with saline followed by 4% depolymerized paraformaldehyde (PFA) in phosphate buffer (0.1 M, pH 7.4). Brains were carefully extracted, post-fixed for 48 h in 4% PFA, thoroughly rinsed, and transferred to phosphate-buffered saline (PBS). Serial 40–50 μm-thick coronal sections were obtained using a Leica VT1000S vibratome (Leica Microsystems, Germany).

2.3 | Immunohistochemistry

The immunofluorescence labeling procedures were performed as described previously (Unal et al. 2015). Briefly, brain sections were rinsed (3 × 10 min) with PBS containing 0.3% Triton-X (PBS-Tx) followed by a 1 h blocking with 20% Normal Horse Serum (NHS) or Normal Goat Serum (NGS) in PBS-Tx at room temperature (RT). The sections were then incubated in PBS-Tx containing the primary antibodies (refer to Table 1) and 1% normal serum for 72 h at 4°C. The sections were then rinsed for 3 × 10 min with PBS-Tx and incubated for 4 h at RT in PBS-Tx containing the secondary antibodies and 1% normal serum. Following the secondary incubation, immunofluorescent sections were rinsed again with PBS-Tx (3 × 10 min) to be mounted and coverslipped using Fluoromount (Thermo Fisher Scientific), and DAB sections were processed as below.

DAB staining was performed with nickel and cobalt intensification. Slices were rinsed in PBS, incubated 30 min in 0.3% hydrogen peroxide to block endogenous peroxidases, and rinsed again 3 × 10 min in PBS. After serum blocking and incubation with primary and secondary antibodies, sections were transferred to DAB solution (0.2 mg/mL DAB, 25 mg/mL ammonium nickel sulfate, 0.4 mg/mL cobalt chloride, 0.4 mg/mL ammonium chloride, 4 mg/mL β-D-glucose in 0.1 M sodium acetate buffer, pH 6.0). The reaction was initiated with glucose oxidase (80–100 μL/50 mL DAB solution) for ~30 min, with solution refreshed every 10 min. The reaction was stopped by rinsing 3 × 5 min in sodium acetate buffer. Sections were then mounted on gelatin-coated slides, dehydrated in ethanol and xylene, and coverslipped with DPX (Fluka).

We used the following secondary antibodies: biotinylated goat anti-rabbit (Vector Laboratories, PK-6101; 1:200), biotinylated horse anti-mouse (Vector Laboratories, PK-6102; 1:200), donkey anti-goat Alexa Fluor 405 (Thermo Fisher Scientific Cat# A48259, RRID:AB_2890272; 1:500), donkey anti-guinea pig Alexa Fluor 488 (Jackson ImmunoResearch Labs Cat# 706-545-148, RRID:AB_2340472; 1:500), and donkey anti-rabbit Alexa Fluor 594 (Thermo Fisher Scientific Cat# A-21207, RRID:AB_141637; 1:500).

2.4 | Microscopy

Microscopic observations and image acquisition were performed using epifluorescence, confocal, and slide-scanning microscopy. Initially, fluorescently labeled sections were examined with an epifluorescence microscope (Olympus BX43) using the Olympus cellSens Imaging Software v2.2. The system was equipped with a monochrome CCD camera (Olympus XM10) and objective lenses of 4x (Plan Apochromat, N.A. = 0.02, Nikon), 10x (Plan Fluor, N.A. = 0.30, Nikon), and 20x (Plan Fluor, N.A. = 0.50, Nikon). Fluorescent signals were detected using three filters, optimized for Alexa Fluor 405 (and DAPI), Alexa Fluor 488, and Alexa Fluor 594. Whole-hemisphere low-magnification images were acquired with the MIA module of Olympus cellSens software.

High-resolution whole-slide images were acquired with a slide-scanning microscope (ZEISS Axio Scan.Z1) at 10x magnification with an Orca Flash 4.0 V3 camera. DAB-stained sections were imaged in bright field with the microscope's LED light source, whereas fluorescence images were acquired using the following excitation/emission parameters: 370–410 nm/430–470 nm (420 nm beamsplitter, 15 ms exposure) for the 405 nm fluorophore; 450–490 nm/500–550 nm (495 nm beamsplitter, 44 ms exposure) for the 488 nm fluorophore; and 538–600 nm/618–756 nm (610 nm beamsplitter, 50 ms exposure) for the 594 nm fluorophore.

Detailed high-resolution observation and imaging of the sections were conducted utilizing Leica SP5 and Leica SP8 confocal microscopes (Leica Microsystems, Wetzlar, Germany) using LAS

TABLE 1 | Primary antibodies.

Molecule	Host species	Dilution	Source, catalogue #	Immunogen
CR	Mouse	1:1000	Swant, CG1	Recombinant human calretinin
CB	Rabbit	1:1000	Swant, CB38	Recombinant rat calbindin D-28k
CB	Mouse	1:1000	Swant, CB300	Whole chicken protein from gut
CaMKIIa	Mouse	1:1000	Abcam, ab22609	Full-length CaMKIIa, clone 6G9
DBH	Rabbit	1:1000	Immunostar, 22806	Bovine DBH
GABA	Rabbit	1:1000	Thermo Fisher, PA5-32241	GABA conjugated to KLH
PV	Guinea Pig	1:1000	Swant, GP72	Recombinant mouse parvalbumin
SCGN	Guinea Pig	1:1000	Synaptic Systems, 436004	Recombinant protein corresponding to AA 1 to 276 from mouse secretagogin
TH	Rabbit	1:1000	Thermo Fisher, OPA1-04050	SDS-denatured, native rat tyrosine hydroxylase purified from pheochromocytoma
TH	Goat	1:1000	Thermo Fisher, OST00324W	Synthetic peptide from aa region 30–100 of human tyrosine hydroxylase conjugated to an immunogenic carrier protein was used as the antigen
TH	Rabbit	1:1000	Sigma, AB152	Denatured tyrosine hydroxylase from rat pheochromocytoma (denatured by sodium dodecyl sulfate).
TH	Mouse	1:25	DSBH, aTH	Recombinant TH (aa 60–368)/beta galactosidase fusion protein

X or LAS AF software. Imaging was conducted with either a 20x (Plan Fluotar, N.A. = 0.4, dry, Leica Microsystems) or a 40x (Plan Apochromat, N.A. = 1.10, water-immersion, Leica Microsystems) objective lens with a minimum resolution of 1024 × 1024 pixels. Fluorescent molecules were excited by the 405 and 635 nm diode lasers, the 477 nm argon laser, and the 552 nm DPSS laser, and were detected by PMT or HyD sensors. The pinhole was set to 1 Airy unit, and for z-stack acquisition, the step size was adjusted to half the optical section thickness. After image acquisition, brightness and contrast were adjusted uniformly across entire images in FIJI (ImageJ; Schindelin et al. 2012), with no non-linear or region-selective modifications applied.

2.5 | Fiber Density Analysis

The NCL is known for having the highest density of TH+ fibers within the pallium. To delineate the NCL in the Japanese quail, we employed a custom software for fiber density analysis (von Eugen et al. 2020). Briefly, images were first cropped to reduce background regions. Residual background signals at the image corners were removed using percentile-based normalization, in which the lowest 0.9% of nonzero intensities were clipped, followed by linear rescaling of intensities to the [0, 1] range. Brain tissue was then extracted using a histogram-based adaptive threshold (typically 0.8 of the normalized intensity range) to separate brain from the background. The resulting binary mask was refined by hole filling and retention of the largest connected component corresponding to the brain region.

To enhance the visualization of fibrous structures, a Jerman vesselness enhancement filter (Jerman et al. 2016) was applied to compute a vesselness probability (local tubularity) map of each 2D image. The parameters were set as $\sigma = 0.5–2.5$ (step = 0.5), spacing = [1, 1], and $\tau = 0.75$. For quantification of local fiber density, the enhanced image was divided into a uniform 100 × 100 grid. Intensity profiles were extracted along horizontal and vertical grid lines to detect fiber-like structures. Baseline correction of each profile was performed using the *msbackadj* function (window size = 20, step size = 20, regression method = spline, smoothing method = expectation–maximization) to remove low-frequency background variations. The corrected signals were subsequently smoothed using robust locally weighted regression (*mslowess*) to minimize noise.

Peak detection was then performed on the smoothed profiles using the *mspeaks* function, with an adaptive threshold determined by Otsu's method to identify local intensity maxima corresponding to individual fibers. The number and positions of detected peaks were calculated within each grid segment for both horizontal and vertical directions. For each grid cell, counts from adjacent horizontal and vertical segments were summed to generate a fiber density map, representing the relative density of fibrous structures across the image. The resulting fiber density map was up-sampled to match the original image resolution for visualization and subsequent quantitative analysis.

To compare TH+ fiber densities between the NCL and other pallial regions, we used the machine learning-based automated image segmentation tool ZEN Intellesis (ZEN 3.7, Zeiss). Images were acquired at 10x magnification using an Axioscan Z1 (Zeiss) equipped with an Orca Flash 4.0 V3 camera. First, regions of interest (ROIs) were manually defined and cropped. A total of 63 ROIs (250 × 250 μm each) were analyzed across all regions. ROIs

were randomly selected from five pallial areas: hyperpallium, mesopallium, NCL, the island fields of the caudal nidopallium, and the auditory area of the nidopallium. Between 10 and 14 images were analyzed per region from two quail brains.

ROIs were then imported into the trainable segmentation module Intellesis (Zeiss). Intellesis performs supervised pixel classification using a random forest-based machine learning algorithm trained on multiscale image features (including intensity, edge, and texture descriptors). A training set of 14 images from different quails was used to train a 64 deep-feature model to recognize TH+ fiber-like structures. During training, fibers were manually annotated to define foreground and background classes. Randomized ROIs from each region were labeled to ensure unbiased model learning. Once training performance was satisfactory, the trained classifier was applied in batch mode to all ROIs for automated segmentation.

Fiber density quantification was performed using the ZEN 3.7 Image Analysis Wizard, calculating the proportion of segmented TH+ area within each ROI. TH+ fiber densities were compared across regions using one-way ANOVA followed by Tukey's multiple comparison test. Statistical analyses and figure generation were conducted in GraphPad Prism (version 10.3.1).

2.6 | Cell Quantification

Cell quantification and colocalization analyses were performed using Cellpose v3.11.0 (Stringer et al. 2020). For each animal, sections containing the VTA and SN were randomly selected for analysis. For CR, six VTA sections and eight SN sections were analyzed. For PV, five VTA sections and five SN sections were analyzed. Images were first cropped to standardized ROIs measuring 500 × 500 μm. Brightness and contrast were adjusted uniformly across comparable images to enhance visualization while preserving relative fluorescence intensity. Processed images were then subjected to automated segmentation using the cyto3 model in Cellpose. For CR and PV detection, the estimated cell diameter was set to 21 pixels, with a flow threshold of 0.4 and a cell probability threshold of 0. For TH, the estimated diameter was set to 31 pixels, with a flow threshold of 0.6 and a cell probability threshold of −1. Segmentation masks were saved as .npy files for subsequent analysis. Total cell counts were determined by extracting unique labeled objects from the mask arrays, excluding background.

Colocalization between CR and TH or PV and TH cells was assessed using a custom-written Python pipeline (Python 3.11; NumPy, Pandas, scikit-image, Matplotlib). For each section and hemisphere, segmentation masks corresponding to each marker were loaded and compared using a fast intersection-over-union (IoU)-based matching approach. Pixelwise intersections between labeled objects were computed, and IoU values were calculated as the ratio of intersection area to union area for each potential object pair. A greedy one-to-one matching algorithm was then applied, ranking candidate pairs by descending IoU score and assigning matches only when IoU ≥ 0.20. Each segmented object was allowed to match only one partner to prevent duplicate assignments. The total number of double-labeled cells and the proportion of CR+ or PV+ cells overlapping with TH+ cells were calculated for each section. For quality control, overlay images were generated in which CR or PV masks were displayed in red, TH masks in cyan, and overlapping regions appeared white. Boundary maps of segmented objects and centroid-based markers for matched cells were also produced to visually verify segmentation accuracy and overlap assignments.

3 | Results

3.1 | Delineation of the Nidopallium in the Japanese Quail

The NCL was defined as the caudal nidopallial region showing the highest density of TH+ fiber labeling together with characteristic TH+ basket-like structures, which have been previously described as distinguishing features of this area (Waldmann and Güntürkün 1993; Wynne and Güntürkün 1995). Three coronal sections from different rostrocaudal levels were analyzed to confirm the consistent presence of these features along the NCL (Figure 1). Anatomical boundaries were delineated based on TH+ fiber distribution and visible landmarks such as the striatum and arcopallial/amygdalar subdivisions. We followed the Avian Brain Nomenclature Forum standards (Jarvis et al. 2005; Reiner et al. 2004) and used the chick brain atlas (Puelles et al. 2018) for orientation.

In the most anterior section (Figure 1A–C), the region of highest TH+ fiber density in the caudal nidopallium was relatively small, yet TH+ basket-like structures were observed coiling around DAPI+ cell bodies. At the mid-level (Figure 1D–F), similar basket-like structures were again found surrounding DAPI+ nuclei. In the most posterior part (Figure 1G–I), these structures were more numerous and prominently distributed within the NCL. Although the NCIF has been reported to contain basket-like structures in other galliform species (von Eugen et al. 2020), we were unable to clearly delineate it from the NCL based on TH labeling in these sections. Together, these findings support a consistent presence of TH+ basket-like structures as a defining feature of the NCL across rostrocaudal levels in the Japanese quail.

3.2 | TH Fiber Density Analysis in the Nidopallium

We generated heatmaps from DAB-stained sections in order to determine the distribution of TH+ fiber densities in the NCL (Figure 2). The schematized and labeled section drawings shown on the right side of Figure 2 were partially based on the chick brain atlas (Puelles et al. 2018). In the more anterior sections (Figure 2A,B), high densities of TH+ fibers were observed in the striatal areas, mesopallium, and hypothalamus. In contrast, the entopallium lacked any TH+ fiber staining at these levels. In the mid-level sections (Figure 2C,D), the dorsal arcopallium exhibited a high density of TH+ fibers, while other regions of the arcopallium/amygdala complex showed relatively low TH+ fiber density. Further posteriorly (Figure 2E,F), the remaining regions of the arcopallium/amygdala complex continued to display similar TH+ fiber densities.

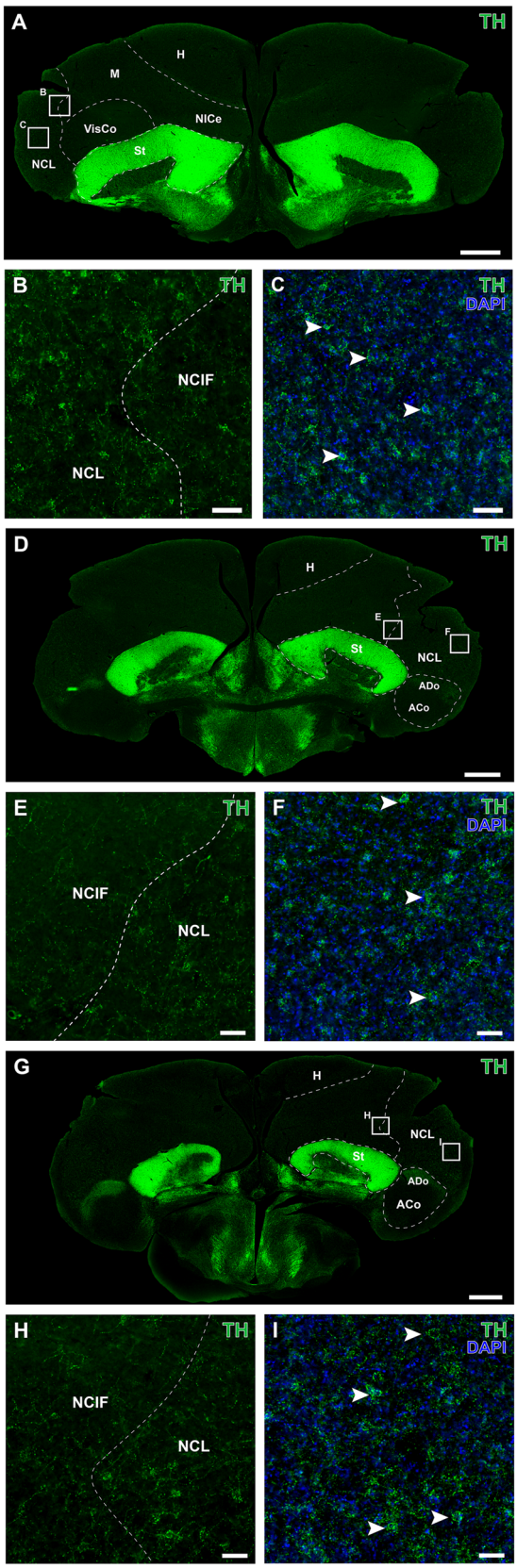

FIGURE 1 | Legend on next page.

FIGURE 1 | TH+ processes and basket-like formations in the NCL. (A, D, G) Slide scan images of three coronal sections at different rostro-caudal levels, from anterior to posterior, with interaural levels based on TH+ fiber distribution and the chick brain atlas (A: 4.72 mm, C: 3.76 mm, E: 3.04 mm). (B, C, E, F, H, I) Magnified views of the boxed regions in the corresponding panels above, with left panels highlighting the NCL border and DAPI staining highlighting basket-like formations (arrowheads). NCL, nidopallium caudolaterale; E, entopallium; M, mesopallium; H, hyperpallium; St, striatum; NICe, nucleus intercollicularis pars externa; NCIF, nidopallium caudolaterale island fields; AD, dorsal arcopallium; AC, commissural arcopallium. Scale bars: 1 mm (A, D, G); 50 μm (B, C, E, F, H, I).

The TH+ fiber-dense lateral structure first appeared in Figure 2B, dorsal to the amygdala, which itself did not display any visible TH+ fibers at that level. In more caudal sections, this area showed increasing TH+ fiber density, extending dorsally and medially from the amygdala toward the dorsomedial part of the section (Figure 2E,F). Based on its alignment with spatial coordinates from the chick brain atlas (Puelles et al. 2018) and previously described TH+ fiber distribution patterns in the avian NCL, this region was identified as the NCL. Although the region appeared relatively uniform, we were able to distinguish the dorsal part of the NCL, characterized by a dense TH+ fiber shell surrounding a fiber-scarce core, consistent with prior reports (Kobylkov et al. 2022). No further subregional differentiation within the NCL was observed.

Additionally, we identified two other regions within the nidopallium. First, the caudomedial nidopallium (NCM) was delineated based on a defined absence of TH+ fibers, situated medially to the striatum as referenced from the chick brain atlas (Puelles et al. 2018). Second, based on the presence of dense TH+ fibers medial to the NCL, we identified the NCIF, a region previously defined in galliform species (von Eugen et al. 2020). Although TH+ fiber density in the NCIF markedly increased at more caudal levels, it remained consistently lower than that observed in the NCL (Figure 2E,F).

After generating heat maps of dopaminergic fiber densities in the Japanese quail pallium, we identified the NCL as the most densely innervated region. Then, we compared TH+ fiber densities across different pallial regions using ZEN Intellesis software to assess whether the NCL is significantly more densely innervated than other regions and to determine whether the remaining regions also exhibit distinct levels of innervation. The average percentage of each region occupied by TH+ fibers across the analyzed sections was calculated and compared (Figure 3). TH+ fibers occupy more than half of the imaged area in the NCL (55.67%), while their density is lower in other regions: 37.06% in the mesopallium, 30.47% in the hyperpallium, 26.87% in the NCIF, and 17.09% in the lateral nidopallium auditory field (AuL). Our analysis, which compares the area occupied by TH+ fibers within predefined regions of the hyperpallium, mesopallium, NCIF, NCL and AuL, showed that pallial regions contain different amounts

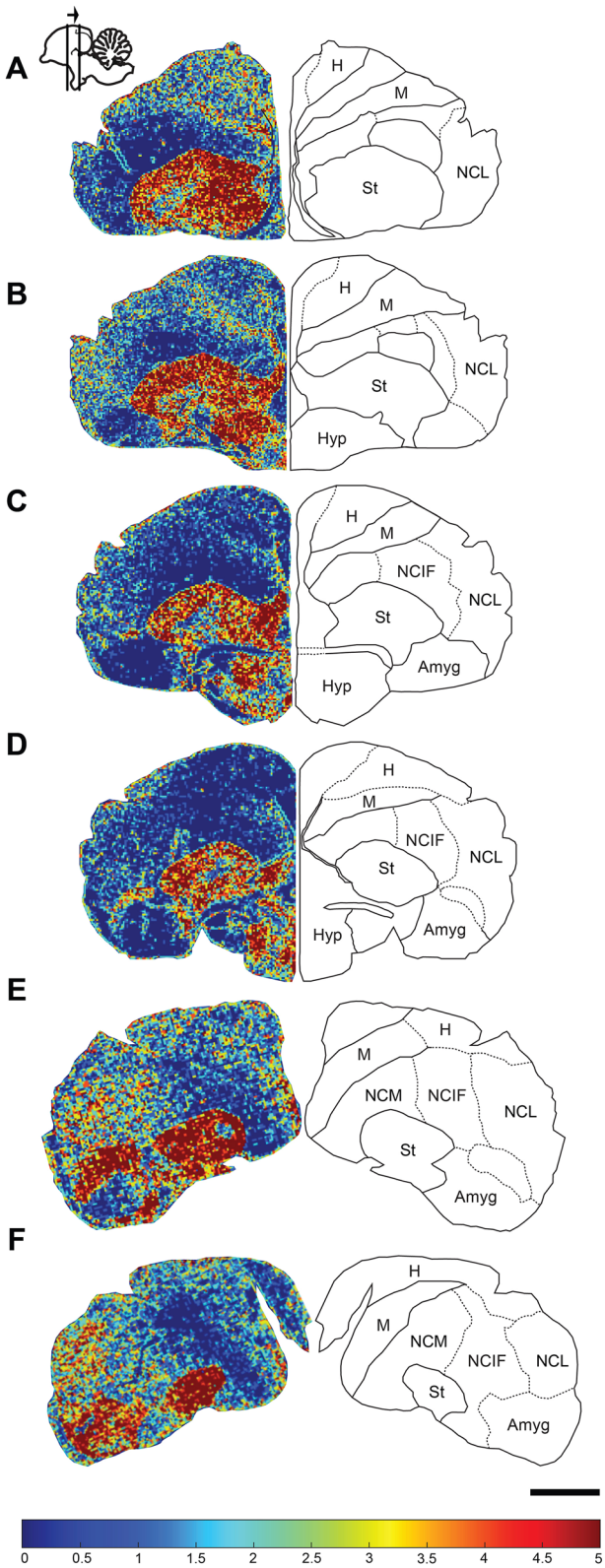

FIGURE 2 | Legend on next page.

of TH+ fibers (one-way ANOVA, $F(4, 58) = 7.861$, $p < 0.0001$; Figure 4). The post hoc analysis (Tukey's multiple comparison test) revealed that the NCL ($M = 139141.51$, $SD = 60105.36$) has higher TH+ innervation, compared to the hyperpallium ($M = 76158.11$, $SD = 40570.85$; $p = 0.0092$), NCIF ($M = 67166.21$, $SD = 33437.94$; $p = 0.0009$), and AuL ($M = 42704.26$, $SD = 20982.81$; $p < 0.0001$). Only the mesopallium ($M = 92632.11$, $SD = 53929.97$) displayed a similarly high level of innervation as the NCL ($p = 0.065$).

3.3 | Postsynaptic Targets of Dopaminergic Projections in the NCL

We investigated the postsynaptic targets of TH+ fibers in the NCL by using immunohistochemistry for different CaBPs and CaMKIIa. We first examined the overall distribution of TH at two rostrocaudal levels and evaluated the labeling patterns of PV and CR, the two major CaBPs in the NCL (Figure 4A–G). Consistent with previous reports in the chick brain, we observed dense TH innervation in striatal regions and the arcopallium with distinct basket-like structures present in the NCL and NCIF (Figure 4A). In contrast, there was no TH innervation in the medial part of the section but a dense projection pattern in the NCL and nidopallium trigeminal projection field (NCT; Figure 4G). Notably, the dorsal amygdalar area, evolutionarily derived from striatal origins, also displays densely packed TH+ fibers.

PV+ cells were markedly more abundant in the NCL and pallial regions in general, compared to CR+ cells. While CR+ cells were identified in the NCM, their presence in the NCL and NCT was sparse. Although both PV and CR staining in the NCL revealed basket-like structures, we could not identify any clear postsynaptic targets within these formations for either CaBP. Nevertheless, PV+ staining revealed a pattern of putative *en passant* TH+ synapses on multiple PV+ cells in the NCL (Figure 4C,F). Although CR+ cells were infrequent in the NCL, some appositions with TH+ fibers were still observed (Figure 4I–L). However, these potential TH+ contacts to CR+ cells were restricted to single boutons rather than the putative *en passant* profiles observed on PV+ cells.

We next carried out a more detailed qualitative analysis of the postsynaptic targets of TH+ fibers in the NCL. For this purpose, we employed additional CaBPs (PV, CR, SCGN, and CB) together with CaMKIIa, a well-established marker of cortical glutamatergic neurons in mammals (Liu and Jones 1996; Figure 5). No PV+ or CR+ cells were located within the TH+ basket-like structures (Figure 5A–F). Potential contacts were therefore limited to PV+ cells apposed to the aforementioned *en passant* TH+ fibers (Figure 5A–C) and CR+ cells contacting individual boutons outside or adjacent to the TH+ basket-like formations (Figure 5D–F). Regarding the other CaBPs, SCGN+ cells were rare throughout the pallial regions, including the NCL (Figure 5H).

FIGURE 2 | TH+ fiber density heatmaps across rostrocaudal levels. (A–F) Representative coronal sections showing TH-immunopositive fiber densities (left) are paired with by corresponding schematized line drawings derived from the heatmap data (right). The color scale represents relative fiber density, with warmer colors indicating higher TH+ fiber concentrations. A schematic brain in the top left illustrates the rostrocaudal levels of the depicted sections. H, hyperpallium; NCM, caudomedial nidopallium; NCIF, nidopallium caudolaterale island fields; NCL, nidopallium caudolaterale; M, mesopallium; St, striatum; Hyp, hypothalamus; Amyg, amygdala. Scale bar: 1 mm.

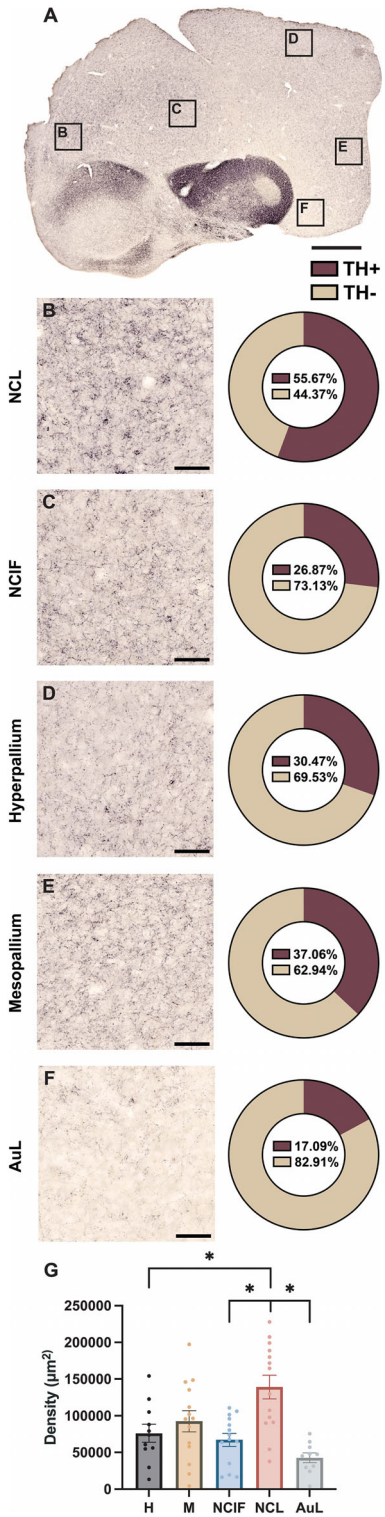

FIGURE 3 | Quantification and comparison of TH+ fiber density across pallial regions. (A) A scanned image of a TH-labeled hemisphere with boxed areas indicating the selected pallial regions. (B–F) Representative 500 × 500 μm images from the NCL, NCIF, hyperpallium (H), mesopallium (M), and lateral nidopallium auditory field (AuL), accompanied by pie charts showing the average proportion of TH+ fiber coverage versus background across all analyzed images for that region. (G) Statistical comparisons of TH+ fiber densities across regions. Error bars represent ± *SEM*, and asterisks denote statistically significant differences ($p < 0.05$). Scale bars: 1000 μm (A); 100 μm (B–F).

A small number of SCGN+ cells were observed to receive sparse contacts from TH+ fibers. CB+ cells were more frequent than CR+ and SCGN+ cells; however, they were not located within the basket-like TH+ structures (Figure 5J–L). As with CR+ and SCGN+ cells, they appeared to receive input from individual TH+ boutons. The only biomarker that clearly labeled neurons within the TH+ basket-like structures was CaMKIIa (Figure 5M–O). CaMKIIa+ cells were also the most abundant among the markers we tested and were consistently enveloped by TH+ basket-like structures, suggesting they may serve as the postsynaptic targets of these specialized TH+ formations.

Finally, we sought to confirm the dopaminergic nature of the TH+ basket-like profiles by distinguishing dopaminergic from noradrenergic fibers using TH+ and DBH+ immunolabeling (Figure 6). Since TH+ fibers include both dopaminergic and noradrenergic populations, whereas DBH+ fibers label only noradrenergic fibers, this comparison allowed us to identify dopaminergic fibers by exclusion. We assessed the presence of basket-like structures in both markers across several pallial regions, including the NCL, NCIF, and NCM. In the NCL, TH+ labeling revealed frequent, characteristic basket-like structures, whereas DBH+ staining showed none, suggesting that these baskets are putatively dopaminergic. Similarly, in the NCIF, a region that also displays dense basket-like structures in chickens, we observed prominent TH+ baskets but no DBH+ counterparts. The NCM lacked both TH+ and DBH+ fibers, consistent with previous findings in other avian species (von Eugen et al. 2020). These results confirm that the basket-like structures observed in the NCL are dopaminergic rather than noradrenergic.

3.4 | Neurochemical Characterization of the Midbrain Dopaminergic System

After confirming through additional DBH labeling that the TH+ fibers in the NCL are dopaminergic rather than noradrenergic, we next investigated their source. We focused on the VTA and SN, two midbrain regions known to give rise to ascending dopaminergic projections in both birds and mammals, to identify the putative origin of TH+ input to the NCL. Consistent with previous observations (Bailhache and Balthazart 1993), both nuclei contained numerous TH+ cell bodies (Figure 7), suggesting that they are the likely source of the dense TH+ innervation observed in the NCL.

To neurochemically characterize TH+ neurons, we quantified their co-expression with PV and CR using automated segmentation followed by IoU-based matching (IoU ≥ 0.20; see Methods). For each section, overlap percentages were calculated by dividing the number of double-labeled cells by the total number of TH+ cells (or CR+/PV+ cells) and multiplying by 100.

In the VTA, PV expression in dopaminergic neurons was negligible. PV+ cells averaged $M = 14.2$ cells ($SD = 14.65$), and TH+ cells averaged $M = 36.0$ cells per section ($SD = 29.32$). The number of PV/TH double-labeled cells was very low ($M = 0.2$ cells per section, $SD = 0.45$), corresponding to a mean overlap of 0.74% of TH cells and 0.69% of PV cells. In the SN, PV/TH overlap remained minimal. PV+ cells averaged $M = 18.25$ cells per section ($SD = 6.70$), and TH+ cells averaged $M = 5.5$ cells per section (SD

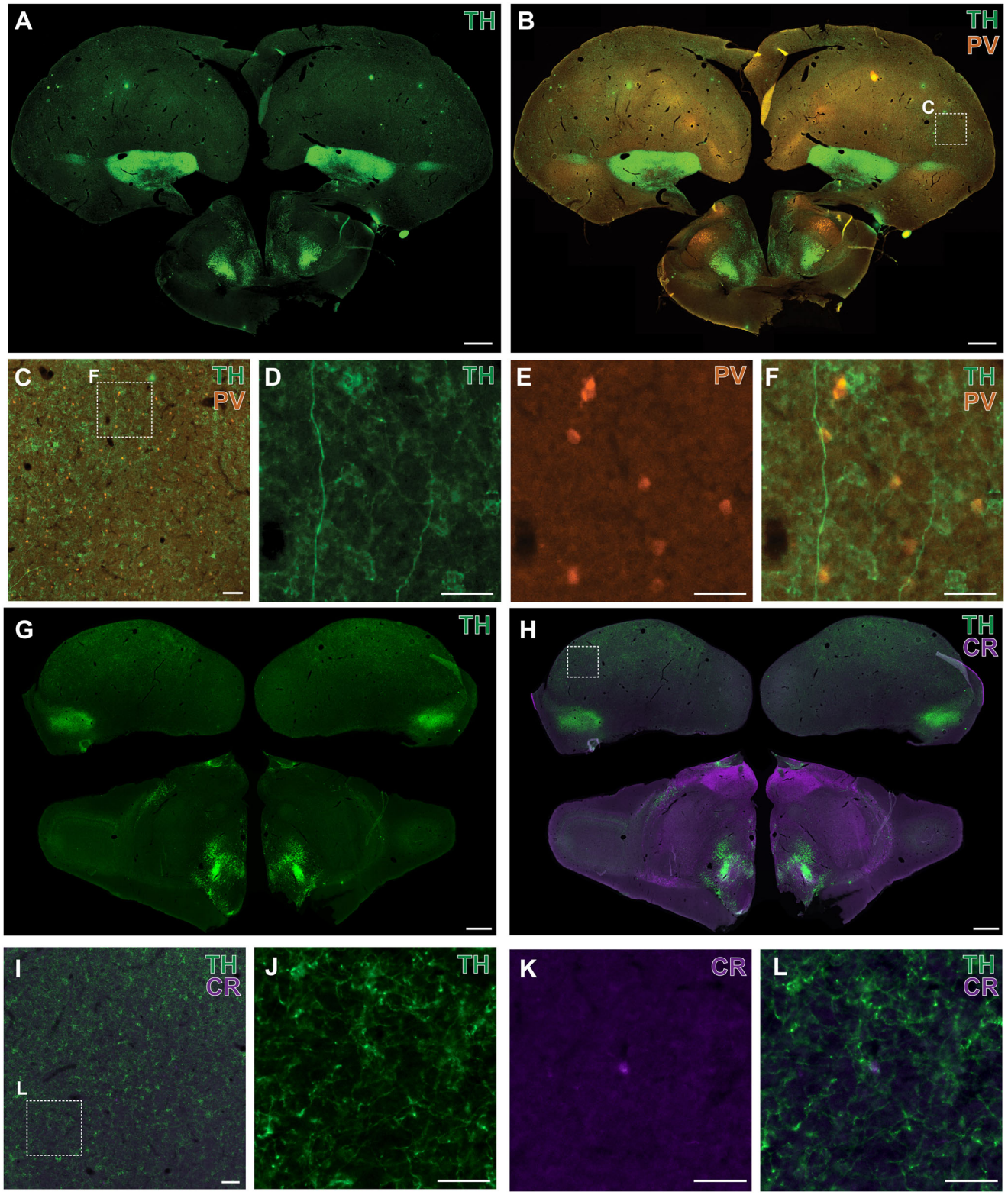

FIGURE 4 | Distribution of TH+ fibers and calcium-binding proteins. (A–B) Coronal brain section immunolabeled for TH (A) and the overlay of TH and PV (B). (C) Enlarged view of the marked region in B showing the overlay in NCL. (D–F) Marked subregion from C showing TH (D) and PV (E) immunolabeling and their overlay (F). (G–H) Coronal brain section immunolabeled for TH (G) and the overlay of TH and CR (H). (I) Enlarged view of the marked region in H depicting the overlay in NCL. (J–L) Enlarged view of the subsection from I showing TH (J) and CR (K) immunolabeling and their overlay (L). Scale bars: 1000 μm (A, B, G, H); 100 μm (C, I); 50 μm (D–F, J–L).

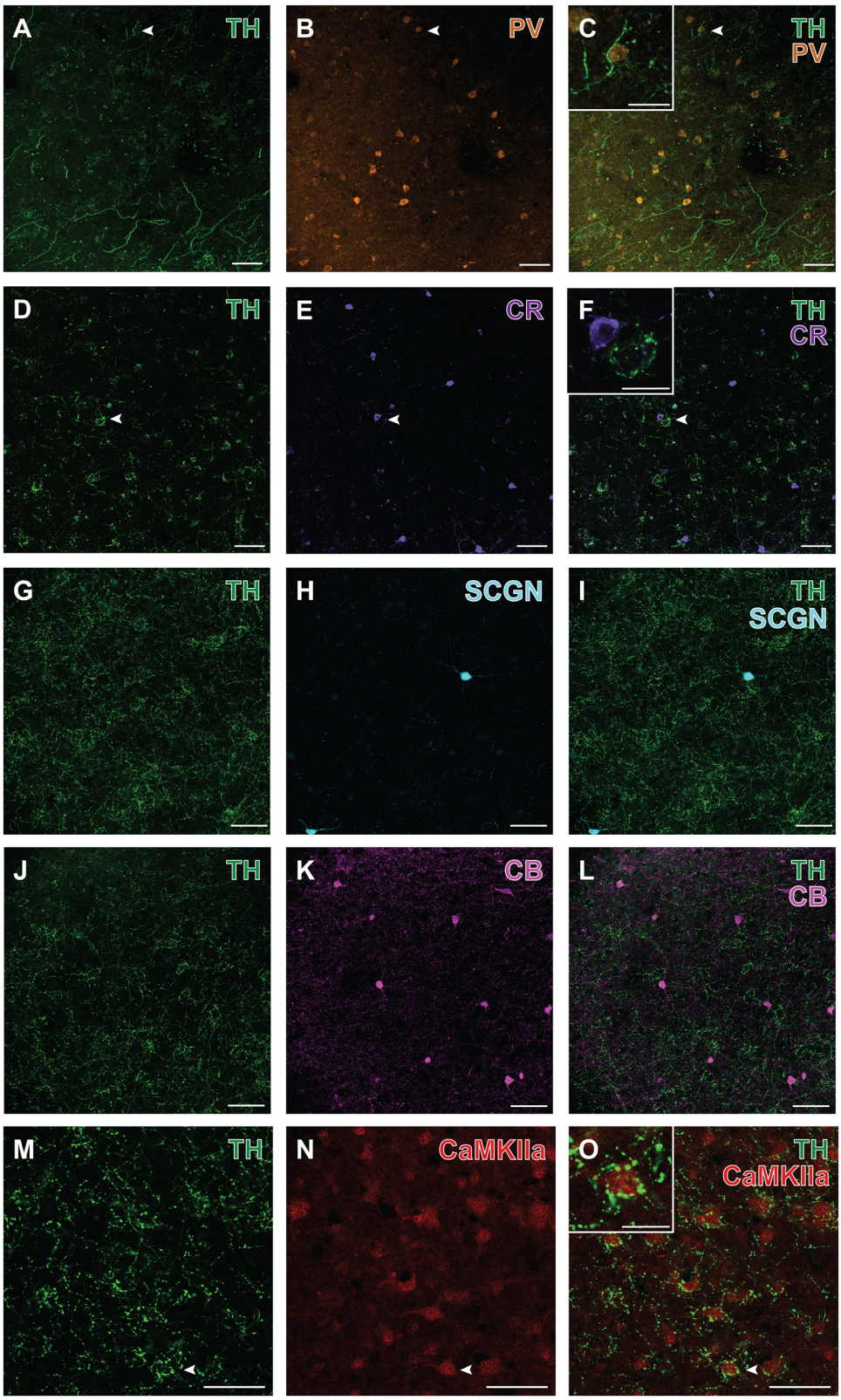

FIGURE 5 | Immunofluorescence labeling of TH with calcium-binding proteins and CaMKIIa. (A–C) Confocal images showing TH (A), PV (B) and their overlay (C), with an arrowhead indicating a PV+ cell adjacent to the TH+ fibers. Inset C provides a close-up of the marked area. (D–F) TH (D), CR (E) and their overlay (F), with an arrowhead marking a CR+ cell near a TH+ basket-like structure. Inset F shows an enlarged view of the marked cell. (G–I) TH (G), SCGN (H) and their overlay (I). (J–L) TH (J), CB (K) and their overlay (L). (M–O) TH (M), CaMKIIa (N) and their overlay (O), with an arrowhead indicating a CaMKIIa+ cell within a TH+ basket-like structure. Inset O shows a close-up of the marked cell. Scale bars: 50 μm (A–O), 20 μm (Insets C, F, O).

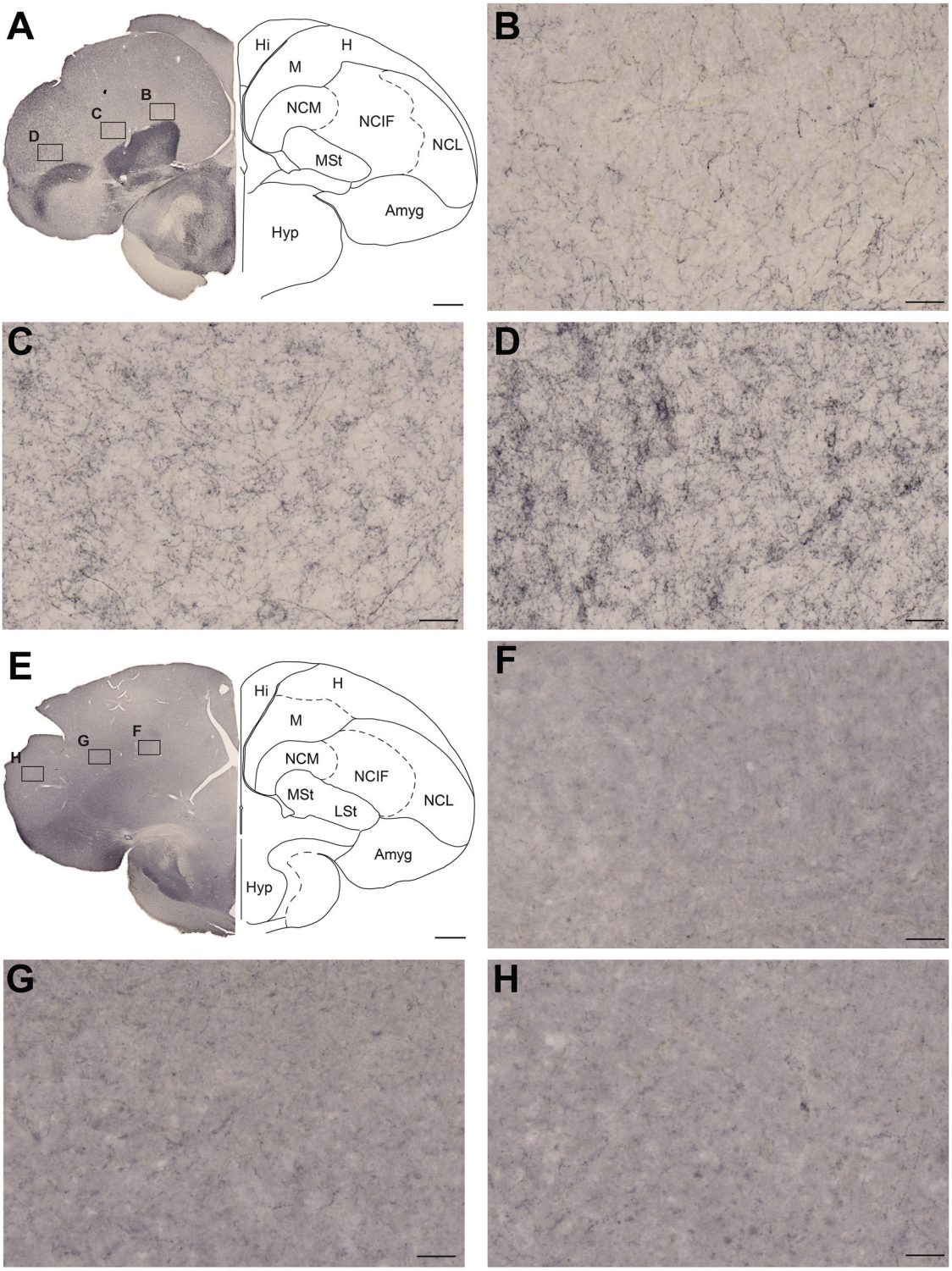

FIGURE 6 | DAB-labeled TH+ and DBH+ fibers in various caudal nidopallium regions. (A) Distribution of TH+ fibers in a coronal brain section of the Japanese quail at interaural level 3.04 mm, with the corresponding chick brain atlas reference shown on the right. (B–D) High-magnification images showing TH+ fiber distribution in the NCM, NCIF, and NCL, respectively. (E) Coronal brain section showing DBH+ fiber distribution at interaural level 3.28 mm, with the corresponding chick brain atlas reference on the right. (F–H) High-magnification views of DBH+ processes in the NCM, NCIF, and NCL, respectively. Hi, hippocampus; H, hyperpallium; NCM, caudomedial nidopallium; NCIF, nidopallium caudolaterale island fields; NCL, nidopallium caudolaterale; M, mesopallium; MSt, medial striatum; LSt, lateral striatum; Hyp, hypothalamus; Amyg, amygdala. Scale bars: 500 μm (A, E); 50 μm (B–D, F–H).

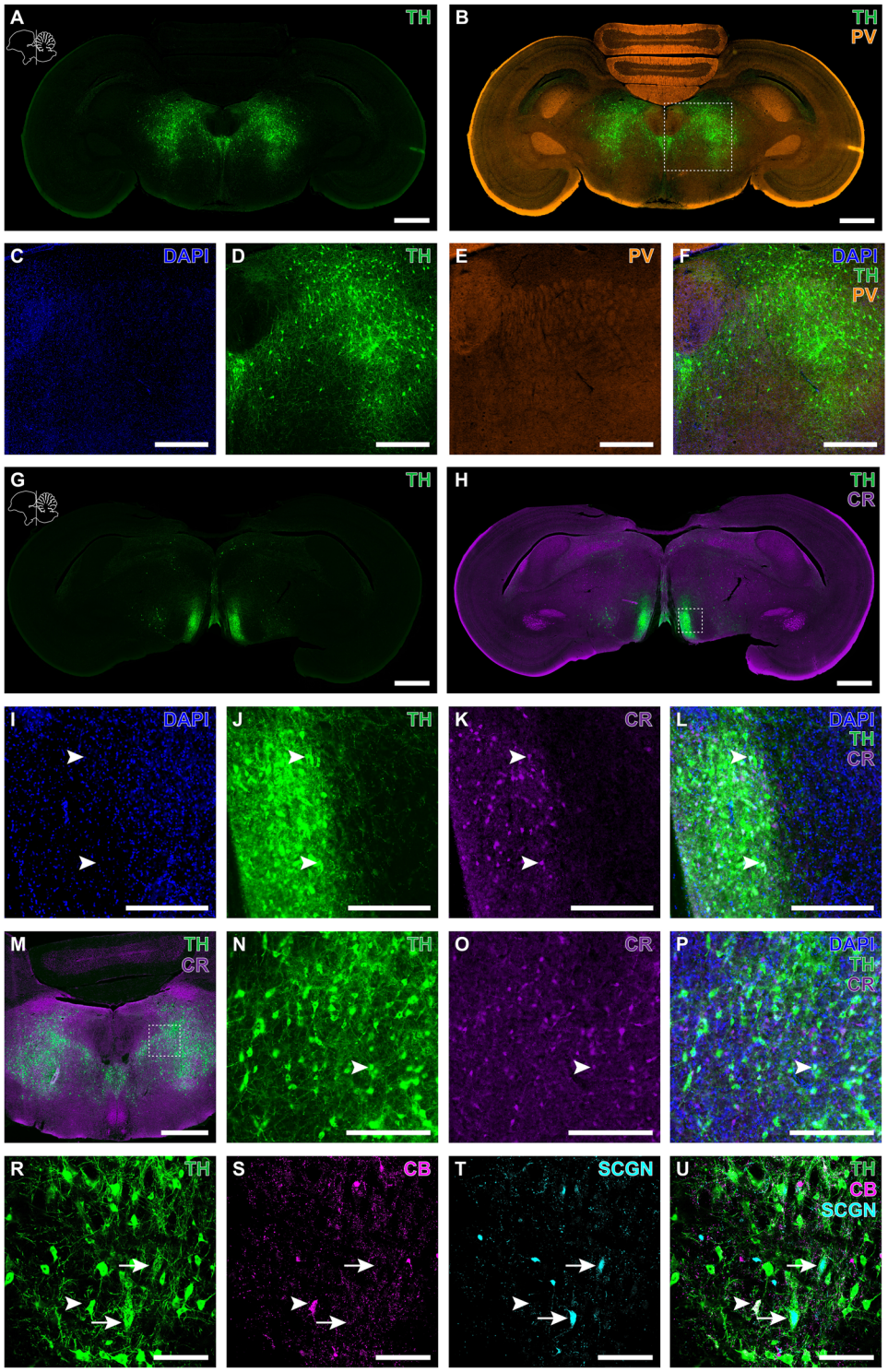

FIGURE 7 | Overlap of TH+ cells with calcium-binding proteins in the VTA and SN. (A, B) Coronal sections from slide scan images showing TH labeling (A) and PV co-labeling (B). (C–F) High-magnification images of the boxed area in B reveal the absence of PV+ cells. (G, H) Coronal slide scanned sections showing TH labeling (G) and CR co-labeling (H). (I–L) High-magnification images of the boxed area in H. (M–P) TH and CR co-labeling in the midbrain, with the boxed area enlarged in N–P. (R–U) Confocal images display midbrain TH+ cells co-expressing CB (S) or SCGN (T), as depicted in the overlay (U). Arrowheads depict TH and CR or CB co-expression while arrows depict TH and SCGN co-expression. Scale bars: 1 mm (A, B, G, H, M); 500 μm (C–F); 250 μm (I–L, N-P); 100 μm (R–U).

= 3.70). The number of double-labeled cells (M = 0.25 cells per section, SD = 0.50) corresponded to a mean overlap of 3.13% of TH cells and 1.32% of PV cells.

In contrast, CR marked a distinct subpopulation of dopaminergic neurons. In the VTA, CR+ cells averaged M = 69.17 cells per section (SD = 26.60), and TH+ cells averaged M = 61.83 cells per section (SD = 44.38). The number of CR/TH double-labeled cells (M = 5.83 cells per section, SD = 5.27) corresponded to a mean overlap of 11.16% of TH cells and 11.33% of CR cells. In the SN, CR+ cells averaged M = 49.75 cells per section (SD = 32.20), and TH+ cells averaged M = 53.88 cells per section (SD = 40.91). CR/TH double-labeled cells averaged M = 4.5 per section (SD = 6.87), corresponding to 5.54% of TH cells and 8.54% of CR cells.

In addition, a small subset of TH+ neurons co-expressed CB, and only sparse SCGN-positive cells were detected within TH+ midbrain regions (Figure 7R–U), indicating minimal overlap for these markers. Together, these results demonstrate that while PV is largely absent and CB and SCGN show only limited co-expression with dopaminergic neurons in the quail midbrain, CR identifies a distinct molecular subset of TH+ neurons in both the VTA and SN.

4 | Discussion

In this study, we provide a comprehensive characterization of the NCL in Japanese quail, focusing on its anatomical boundaries, neurochemical architecture, and dopaminergic innervation. We first delineated the NCL using TH+ basket structures as a marker and quantified their distribution with a custom fiber density analysis, providing an objective basis for defining this pallial region. Building on this structural framework, we examined the putative postsynaptic targets of these TH+ fibers by combining a panel of cellular markers, including PV, CB, CR, SCGN, and CaMKIIa, with detailed mapping of CaBPs within the NCL. Finally, we traced the source of dopaminergic input to the VTA and characterized these neurons using the same biomarkers. Together, these data provide new insights into the organization of avian associative pallial circuits, highlighting both conserved features and interspecific differences of dopaminergic modulation that may underlie complex cognitive processes in birds.

4.1 | NCL Delineation

Consistent with findings in pigeons, carrion crows, zebra finches, chickens, and blackcaps (Kobylkov et al. 2022; von Eugen et al. 2020; Waldmann and Güntürkün 1993; Wynne and Güntürkün 1995), the NCL was defined as the area with the densest TH+ innervation and basket formations. TH immunolabeling revealed a dense plexus of fibers concentrated within the NCL, contributing to the view that this region functions as a major hub for executive and associative processes in birds (Güntürkün 2005b).

Along the rostrocaudal axis, the NCL gradually decreases in size, a pattern also observed in other avian species (Kobylkov et al. 2022; von Eugen et al. 2020). To quantitatively support these boundaries, we generated coronal heat maps from six rostrocaudal levels using custom software that converts immunolabeled sections into fiber density maps, a method previously applied in other birds (Kobylkov et al. 2022; von Eugen et al. 2020). These analyses confirmed the NCL boundaries and revealed additional pallial subdivisions. Applying the subdivision scheme proposed by Kobylkov et al. (2022), we identified the dorsal subdivision of the NCL, whereas other subdivisions could not be reliably distinguished. This partial delineation suggests that some NCL subdivisions may be less anatomically distinct in quail than in pigeons or chickens, underscoring interspecific differences in pallial anatomy.

Quantitative analysis of TH+ fiber densities across pallial regions confirmed the prominent innervation of the NCL. We measured the proportion of each region occupied by TH+ fibers in predefined areas and found that the NCL contained the highest density, followed by the mesopallium, hyperpallium, NCIF, and AuL. These results provide quantitative evidence that the NCL is the primary TH+ target in the quail pallium and underscore regional heterogeneity in catecholaminergic input. Interestingly, whereas previous studies reported a high density of TH+ fibers in the NCM (Kobylkov et al. 2022; Maney and Pinaud 2011; von Eugen et al. 2020), we observed that this structure contains almost none in the Japanese quail. This finding suggests interspecific differences in dopaminergic innervation of auditory-associative areas, which may be linked to variation in sensory processing or learning strategies between quail and songbirds (Maney and Pinaud 2011; Pinaud and Mello 2007).

Comparative analysis also revealed that other pallial regions display divergent TH+ patterns. The sensorimotor arcopallium exhibited dense TH+ fiber labeling, consistent with findings in other avian species, potentially reflecting its role in motor and associative circuits. In contrast, the amygdala (including the nucleus taeniae and posterolateral amygdalar regions) appeared largely devoid of TH+ fibers in some areas, whereas other subdivisions of the arcopallium/amygdala complex showed a dense TH+ fiber pattern. Together, these patterns reinforce the notion that dopaminergic innervation in avian pallium is highly region-specific, supporting distinct functional roles of each area.

4.2 | Putative Postsynaptic Targets of the TH+ Baskets in NCL

Findings of this study show that dopaminergic TH+ basket-like structures in the NCL predominantly target CaMKIIa+ neurons, while putative GABAergic interneurons marked by PV, CR, CB, or SCGN may receive only sparse *en passant* contacts or individual synaptic boutons. The consistent envelopment of CaMKIIa+ neurons by TH+ baskets suggests that dopaminergic inputs primarily influence excitatory pathways, as first proposed by Durstewitz et al. (1998). This organization parallels the mammalian PFC, where dopamine modulates pyramidal neurons to regulate working memory, attention, and decision-making (Durstewitz et al. 1999; Ott and Nieder 2019). By directly modulating projection neurons, dopamine in the Japanese quail NCL may enhance signal-to-noise ratios and facilitate flexible rule learning, consistent with lesion studies indicating that NCL integrity is essential for adaptive decision-making (Hartmann and Güntürkün 1998; Mogensen and Divac 1993).

Our results also indicate that dopaminergic fibers in the NCL also likely contact GABAergic interneurons, although sparsely and without forming basket-like structures. The appositions we observed suggest that inhibitory circuits may still be modulated by dopamine, but in a more diffuse manner than excitatory projection neurons. This contrasts with the mammalian PFC, where certain interneuron types, including PV+ fast-spiking cells, are prominent targets of dopaminergic input and contribute to network oscillations (Spool et al. 2021; Zaremba et al. 2025). In avian species, the functional consequences of these limited interneuron contacts remain unclear, but they may provide subtle modulation of inhibitory tone rather than direct gating of NCL output. Overall, TH+ baskets around CaMKIIa+ neurons, alongside sparse interneuron contacts, position the NCL as a dopaminergic hub specialized for modulating excitatory circuits. This arrangement may reflect an evolutionary adaptation for efficient executive processing in birds, highlighting both shared and distinct features compared with the mammalian PFC.

4.3 | Dopaminergic Projections From the VTA and SN

The midbrain dopaminergic system has mostly been studied in songbirds, often in relation to song learning (Duffy et al. 2022; Gadagkar et al. 2016; Xiao et al. 2018). Song learning relies on complex motor skills and social interactions, with midbrain dopaminergic neurons directly modulating the song nuclei that underlie these behaviors (Duffy et al. 2022; Gadagkar et al. 2016; Hara et al. 2007; Kubikova and Košťál 2009; Person et al. 2008; Xiao et al. 2018). Yet, in non-songbird avian species and mammals, midbrain dopaminergic neurons also modulate motor and cognitive regions, shaping a wide range of appetitive and aversive behaviors, while contributing to different forms of learning and memory (Durstewitz et al. 1999; Smeets et al. 2000).

In contrast to birds, the co-expression of CaBPs in midbrain dopaminergic structures has been extensively studied in mammals (Fu et al. 2012; Liang et al. 1996; Mcritchie et al. 1996). CaBPs serve as valuable markers for distinguishing neuronal subpopulations with distinct electrophysiological, morphological, or cellular properties (Mcritchie et al. 1996). For example, dopaminergic neurons expressing CB or CR appear more resistant to neurodegenerative diseases such as Parkinson's (del Rey et al. 2024; Fairless et al. 2019; Mouatt-Prigent et al. 1994). To address this gap in avian research, studies examining CaBPs in midbrain dopaminergic neurons have so far been limited to zebra finches (Mitra et al. 2022). In the present study, focusing on the NCL of the Japanese quail, we expanded this literature by analyzing CaBP expression in dense TH+ midbrain regions—the presumed source of the fibers used to delineate the NCL. Specifically, we performed CB, CR, PV, and SCGN labeling in these regions.

We found that CR was most abundant among the examined CBPs in the midbrain dopaminergic regions of the Japanese quail, with some CR cells overlapping with TH+ cells (11% in VTA and 6% in SN). This overlap appeared both in anterior sections of the VTA and in posterior sections of the SN. In addition, as in the zebra finch (Mitra et al. 2022), CR-positive cells showed a more circular shape, compared to CB+ and SCGN+ neurons. These similarities suggest that the CR+ VTA/SN neurons may represent a comparable neuronal population in these two distantly related bird species.

SCGN+ and CB+ cells were also present in midbrain dopaminergic regions, albeit at lower frequencies than CR-immunopositive cells. While SCGN expression has previously been reported in the VTA of chickens (Zahola et al. 2019), we found that some SCGN+ cells in Japanese quail co-express TH. Interestingly, in these SCGN+/TH+ cells, TH expression appeared weaker and patchier. Mitra et al. (2022) classified VTA and SN cells in zebra finches into three subtypes based on TH expression intensity and reported no SCGN expression in TH cells. In contrast, in Japanese quail, SCGN expression may occur in cells corresponding to subtype 1 or 2 of their classification, which are characterized by weak TH expression.

Finally, we did not detect any PV+ cell bodies in the VTA and SN, whereas PV-positive cells were present in the cerebellum within the same section, as anticipated (Rogers 1989). Automated cell quantification further confirmed that overlap between PV and TH was negligible in both regions. This finding indicates that the Japanese quail differs from the zebra finch, a songbird, where PV-positive as well as PV- and TH-co-expressing cells have been reported in both the VTA and SN (Mitra et al. 2022).

4.4 | Conclusion

Our study provides a detailed anatomical and neurochemical characterization of the Japanese quail NCL, revealing a selective dopaminergic innervation that predominantly targets excitatory projection neurons while largely sparing GABAergic interneurons. This organization highlights the NCL's role as a hub for dopaminergic modulation of executive circuits, analogous in part to the mammalian PFC, yet with interspecific differences in interneuron involvement and regional innervation patterns. By mapping midbrain dopaminergic inputs and identifying their CaBP profiles, we establish a framework for linking specific dopaminergic subpopulations to their postsynaptic targets within the NCL. These findings advance our understanding of avian associative pallial circuits and their functional parallels to the mammalian PFC, providing a foundation for future studies dissecting the role of selective dopaminergic pathways in cognition and behavior. Ultimately, our work emphasizes both conserved principles and evolutionary specializations of neuromodulatory systems across vertebrates, offering a framework for comparative studies of executive function and its neural substrates.

Acknowledgments

The authors have nothing to report.

Funding

This work was supported by the Scientific and Technological Research Council of Türkiye (TÜBİTAK; Project No. 123K557 to GU), Deutsche Forschungsgemeinschaft (DFG; Project No. 395940726/SFB1372 to OG), and the TÜBİTAK-Deutscher Akademischer Austauschdienst (DAAD) Joint Project (TÜBİTAK Project No. 123N516; DAAD Project No. 57685578 to GU and NR).

Data Availability Statement

The data that support the findings of this study are available from the corresponding author upon reasonable request.

References

Akins, C., M. Domjan, and G. G.-J. Experimental. 1994. "Topography of Sexually Conditioned Behavior in Male Japanese Quail (*Coturnix japonica*) Depends on the CS–US Interval." *Journal of Experimental Psychology: Animal Behavior Processes* 20, no. 2: 199–209. https://doi.org/10.1037/0097-7403.20.2.199.

Bailhache, T., and J. Balthazart. 1993. "The Catecholaminergic System of the Quail Brain: Immunocytochemical Studies of Dopamine β-Hydroxylase and Tyrosine Hydroxylase." *Journal of Comparative Neurology* 329, no. 2: 230–256. https://doi.org/10.1002/CNE.903290206.

Ball, G., and J. Balthazart. 2010. "Japanese Quail as a Model System for Studying the Neuroendocrine Control of Reproductive and Social Behaviors." *ILAR Journal* 51, no. 4: 310–325. https://academic.oup.com/ilarjournal/article-abstract/51/4/310/676047.

Benton, M. J., and P. C. J. Donoghue. 2007. "Paleontological Evidence to Date the Tree of Life." *Molecular Biology and Evolution* 24, no. 1: 26–53. https://doi.org/10.1093/MOLBEV/MSL150.

Billings, B. K., A. Bhagwandin, N. Patzke, et al. 2020. "Nuclear Organization and Morphology of Catecholaminergic Neurons and Certain Pallial Terminal Networks in the Brain of the Nile Crocodile, *Crocodylus niloticus*." *Journal of Chemical Neuroanatomy* 109: 101851. https://doi.org/10.1016/J.JCHEMNEU.2020.101851.

Bolnick, D. I., R. D. H. Barrett, K. B. Oke, D. J. Rennison, and Y. E. Stuart. 2018. "(Non)Parallel Evolution." *Annual Review of Ecology, Evolution, and Systematics* 49: 303–330. https://doi.org/10.1146/ANNUREV-ECOLSYS-110617-062240/CITE/REFWORKS.

Colquitt, B. M. 2022. "Organizational Conservation and Flexibility in the Evolution of Birdsong and Avian Motor Control." *Brain, Behavior and Evolution* 97, no. 5: 255–264. https://doi.org/10.1159/000525019.

del Rey, N. L. G., N. Hernández-Pinedo, M. Carrillo, et al. 2024. "Calbindin and Girk2/Aldh1a1 Define Resilient vs Vulnerable Dopaminergic Neurons in a Primate Parkinson's Disease Model." *Npj Parkinson's Disease* 10, no. 1: 1–15. https://doi.org/10.1038/S41531-024-00777-0;SUBJMETA.

Divac, I., J. Mogensen, and A. Björklund. 1985. "The Prefrontal 'Cortex' in the Pigeon. Biochemical Evidence." *Brain Research* 332, no. 2: 365–368. https://doi.org/10.1016/0006-8993(85)90606-7.

Domjan, M., R. Lyons, N. C. North, and J. Bruell. 1986. "Sexual Pavlovian Conditioned Approach Behavior in Male Japanese Quail (*Coturnix japonica*)." *Journal of Comparative Psychology* 100, no. 4: 413–421. https://doi.org/10.1037/0735-7036.100.4.413.

Domjan, M., D. O'Vary, and P. Greene. 1988. "Conditıoning of Appetitive and Consummatory Sexual Behavior in Male Japanese Quail." *Journal of the Experimental Analysis of Behavior* 50, no. 3: 505–519. https://doi.org/10.1901/JEAB.1988.50-505.

Duffy, A., K. W. Latimer, J. H. Goldberg, A. L. Fairhall, and V. Gadagkar. 2022. "Dopamine Neurons Evaluate Natural Fluctuations in Performance Quality." *Cell Reports* 38, no. 13: 110574. https://doi.org/10.1016/j.celrep.2022.110574.

Durstewitz, D., S. Kröner, and O. Güntürkün. 1999. "The Dopaminergic Innervation of the Avian Telencephalon." *Progress in Neurobiology* 59, no. 2: 161–195. https://doi.org/10.1016/S0301-0082(98)00100-2.

Durstewitz, D., S. Kröner, H. C. Hemmings, and O. Güntürkün. 1998. "The Dopaminergic Innervation of the Pigeon Telencephalon: Distribution of DARPP-32 and Co-Occurrence With Glutamate Decarboxylase and Tyrosine Hydroxylase." *Neuroscience* 83, no. 3: 763–779. https://doi.org/10.1016/S0306-4522(97)00450-8.

Durstewitz, D., and J. K. Seamans. 2002. "The Computational Role of Dopamine D1 Receptors in Working Memory." *Neural Networks* 15, no. 4-6: 561–572. https://doi.org/10.1016/s0893-6080(02)00049-7.

Fairless, R., S. K. Williams, and R. Diem. 2019. "Calcium-Binding Proteins as Determinants of Central Nervous System Neuronal Vulnerability to Disease." *International Journal of Molecular Sciences* 20, no. 9: 2146. https://doi.org/10.3390/IJMS20092146.

Fu, Y. H., Y. Yuan, G. Halliday, Z. Rusznák, C. Watson, and G. Paxinos. 2012. "A Cytoarchitectonic and Chemoarchitectonic Analysis of the Dopamine Cell Groups in the Substantia Nigra, Ventral Tegmental Area, and Retrorubral Field in the Mouse." *Brain Structure and Function* 217, no. 2: 591–612. https://doi.org/10.1007/S00429-011-0349-2.

Gadagkar, V., P. A. Puzerey, R. Chen, E. Baird-Daniel, A. R. Farhang, and J. H. Goldberg. 2016. "Dopamine Neurons Encode Performance Error in Singing Birds." *Science* 354, no. 6317: 1278–1282. https://doi.org/10.1126/science.aah6837.

Güntürkün, O. 2005a. "Avian and Mammalian "Prefrontal Cortices": Limited Degrees of Freedom in the Evolution of the Neural Mechanisms of Goal-State Maintenance." *Brain Research Bulletin* 66, no. 4-6: 311–316. https://doi.org/10.1016/J.BRAINRESBULL.2005.02.004.

Güntürkün, O. 2005b. "The Avian 'Prefrontal Cortex' and Cognition." *Current Opinion in Neurobiology* 15, no. 6: 686–693. https://doi.org/10.1016/J.CONB.2005.10.003.

Güntürkün, O. 2012. "The Convergent Evolution of Neural Substrates for Cognition." *Psychological Research* 76, no. 2: 212–219. https://doi.org/10.1007/S00426-011-0377-9/FIGURES/3.

Güntürkün, O., and T. Bugnyar. 2016. "Cognition Without Cortex." *Trends in Cognitive Sciences* 20, no. 4: 291–303. https://doi.org/10.1016/J.TICS.2016.02.001.

Güntürkün, O., K. von Eugen, J. Packheiser, and R. Pusch. 2021. "Avian Pallial Circuits and Cognition: A Comparison to Mammals." *Current Opinion in Neurobiology* 71: 29–36. https://doi.org/10.1016/J.CONB.2021.08.007.

Gutiérrez, G., and M. Domjan. 1997. "Differences in the Sexual Conditioned Behavior of Male and Female Japanese Quail (*Coturnix japonica*)." *Journal of Comparative Psychology* 111, no. 2: 135–142. https://doi.org/10.1037/0735-7036.111.2.135.

Hara, E., L. Kubikova, N. A. Hessler, and E. D. Jarvis. 2007. "Role of the Midbrain Dopaminergic System in Modulation of Vocal Brain Activation by Social Context." *European Journal of Neuroscience* 25, no. 11: 3406–3416. https://doi.org/10.1111/J.1460-9568.2007.05600.X.

Hartmann, B., and O. Güntürkün. 1998. "Selective Deficits in Reversal Learning After Neostriatum Caudolaterale Lesions in Pigeons: Possible Behavioral Equivalencies to the Mammalian Prefrontal System." *Behavioural Brain Research* 96, no. 1-2: 125–133. https://doi.org/10.1016/S0166-4328(98)00006-0.

Herold, C., N. Palomero-Gallagher, B. Hellmann, et al. 2011. "The Receptor Architecture of the Pigeons' Nidopallium Caudolaterale: An Avian Analogue to the Mammalian Prefrontal Cortex." *Brain Structure & Function* 216, no. 3: 239–254. https://doi.org/10.1007/S00429-011-0301-5.

Jarvis, E. D., O. Güntürkün, L. Bruce, et al. 2005. "Avian Brains and a New Understanding of Vertebrate Brain Evolution." *Nature Reviews Neuroscience* 6, no. 2: 151–159. https://doi.org/10.1038/NRN1606.

Jerman, T., F. Pernus, B. Likar, and Z. Spiclin. 2016. "Enhancement of Vascular Structures in 3D and 2D Angiographic Images." *IEEE Transactions on Medical Imaging* 35, no. 9: 2107–2118. https://doi.org/10.1109/TMI.2016.2550102.

Kalenscher, T., B. Diekamp, and O. Güntürkün. 2003. "Neural Architecture of Choice Behaviour in a Concurrent Interval Schedule." *European Journal of Neuroscience* 18, no. 9: 2627–2637. https://doi.org/10.1046/J.1460-9568.2003.03006.X.

Kobylkov, D., I. Musielak, K. Haase, et al. 2022. "Morphology of the "Prefrontal" Nidopallium Caudolaterale in the Long-Distance Night-Migratory Eurasian Blackcap (*Sylvia atricapilla*)." *Neuroscience Letters* 789: 136869. https://doi.org/10.1016/J.NEULET.2022.136869.

Kocourek, M., Y. Zhang, L. Sandberg, et al. 2025. "Cellular Scaling Rules for Brains of the Galliform Birds (Aves, Galliformes) Compared to Those of Songbirds and Parrots: Distantly Related Avian Lineages Have Starkly Different Neuronal Cerebrotypes." *Brain, Behavior and Evolution* 100, no. 3: 183–199. https://doi.org/10.1159/000545417.

Kubikova, Ľ., and Ľ. Košťál. 2009. "Dopaminergic System in Birdsong Learning and Maintenance." *Journal of Chemical Neuroanatomy* 39, no. 2: 112–123. https://doi.org/10.1016/J.JCHEMNEU.2009.10.004.

Kubikova, L., K. Wada, and E. D. Jarvis. 2010. "Dopamine Receptors in a Songbird Brain." *Journal of Comparative Neurology* 518, no. 6: 741–769. https://doi.org/10.1002/CNE.22255.

Kuenzel, W. J., L. Medina, A. Csillag, D. J. Perkel, and A. Reiner. 2011. "The Avian Subpallium: New Insights Into Structural and Functional Subdivisions Occupying the Lateral Subpallial Wall and Their Embryological Origins." *Brain Research* 1424: 67–101. https://doi.org/10.1016/J.BRAINRES.2011.09.037.

Lee, S. H., A. C. Kwan, S. Zhang, et al. 2012. "Activation of Specific Interneurons Improves V1 Feature Selectivity and Visual Perception." *Nature* 488, no. 7411: 379–383. https://doi.org/10.1038/NATURE11312.

Liang, C. L., C. M. Sinton, and D. C. German. 1996. "Midbrain Dopaminergic Neurons in the Mouse: Co-Localization With Calbindin-D28k and Calretinin." *Neuroscience* 75, no. 2: 523–533. https://doi.org/10.1016/0306-4522(96)00228-X.

Lissek, S., B. Diekamp, and O. Güntürkün. 2002. "Impaired Learning of a Color Reversal Task After NMDA Receptor Blockade in the Pigeon (*Columba livia*) Associative Forebrain (Neostriatum Caudolaterale)." *Behavioral Neuroscience* 116, no. 4: 523–529. https://doi.org/10.1037/0735-7044.116.4.523.

Liu, X. B., and E. G. Jones. 1996. "Localization of Alpha Type II Calcium Calmodulin-Dependent Protein Kinase at Glutamatergic but Not γ-Aminobutyric Acid (GABAergic) Synapses in Thalamus and Cerebral Cortex." *Proceedings of the National Academy of Sciences of the United States of America* 93, no. 14: 7332–7336. https://doi.org/10.1073/PNAS.93.14.7332.

Maney, D., and R. Pinaud. 2011. "Estradiol-Dependent Modulation of Auditory Processing and Selectivity in Songbirds." *Frontiers in Neuroendocrinology* 32, no. 3: 287–302. https://doi.org/10.1016/J.YFRNE.2010.12.002.

McCasland, J. S., and L. S. Hibbard. 1997. "GABAergic Neurons in Barrel Cortex Show Strong, Whisker-Dependent Metabolic Activation During Normal Behavior." *Journal of Neuroscience* 17, no. 14: 5509–5527. https://doi.org/10.1523/JNEUROSCI.17-14-05509.1997.

Mcritchie, D. A., C. D. Hardman, and G. M. Halliday. 1996. "Cytoarchitectural Distribution of Calcium Binding Proteins in Midbrain Dopaminergic Regions of Rats and Humans." *Journal of Comparative Neurology* 364: 121–150. https://doi.org/10.1002/(SICI)1096-9861(19960101)364:1.

Mitra, S., S. Basu, O. Singh, A. Srivastava, and P. S. Singru. 2022. "Calcium-Binding Proteins Typify the Dopaminergic Neuronal Subtypes in the Ventral Tegmental Area of Zebra Finch, *Taeniopygia guttata*." *Journal of Comparative Neurology* 530, no. 14: 2562–2586. https://doi.org/10.1002/CNE.25352.

Mogensen, J., and I. Divac. 1982. "The Prefrontal "Cortex" in the Pigeon. Behavioral Evidence." *Brain, Behavior and Evolution* 21, no. 2-3: 60–66. https://doi.org/10.1159/000121617.

Mogensen, J., and I. Divac. 1993. "Behavioural Effects of Ablation of the Pigeon-Equivalent of the Mammalian Prefrontal Cortex." *Behavioural Brain Research* 55, no. 1: 101–107. https://doi.org/10.1016/0166-4328(93)90012-F.

Mouatt-Prigent, A., Y. Agid, and E. C. Hirsch. 1994. "Does the Calcium Binding Protein Calretinin Protect Dopaminergic Neurons Against Degeneration in Parkinson's Disease?" *Brain Research* 668, no. 1-2: 62–70. https://doi.org/10.1016/0006-8993(94)90511-8.

Nomura, T., M. Takahashi, Y. Hara, and N. Osumi. 2008. "Patterns of Neurogenesis and Amplitude of Reelin Expression Are Essential for Making a Mammalian-type Cortex." *PLoS ONE* 3, no. 1: e1454. https://doi.org/10.1371/journal.pone.0001454.

Ott, T., and A. Nieder. 2019. "Dopamine and Cognitive Control in Prefrontal Cortex." *Trends in Cognitive Sciences* 23, no. 3: 213–234. https://doi.org/10.1016/j.tics.2018.12.006.

Ottinger, M. A., N. Thompson, C. Viglietti-Panzica, and G. C. Panzica. 1997. "Neuroendocrine Regulation of GnRH and Behavior During Aging in Birds." *Brain Research Bulletin* 44, no. 4: 471–477. https://doi.org/10.1016/S0361-9230(97)00228-1.

Person, A. L., S. D. Gale, M. A. Farries, and D. J. Perkel. 2008. "Organization of the Songbird Basal Ganglia, Including Area X." *Journal of Comparative Neurology* 508, no. 5: 840–866. https://doi.org/10.1002/CNE.21699.

Pika, S., M. J. Sima, C. R. Blum, E. Herrmann, and R. Mundry. 2020. "Ravens Parallel Great Apes in Physical and Social Cognitive Skills." *Scientific Reports* 10, no. 1: 1–19. https://doi.org/10.1038/S41598-020-77060-8.

Pinaud, R., and C. V. Mello. 2007. "GABA Immunoreactivity in Auditory and Song Control Brain Areas of Zebra Finches." *Journal of Chemical Neuroanatomy* 34, no. 1-2: 1–21. https://doi.org/10.1016/J.JCHEMNEU.2007.03.005.

Prum, R. O., J. S. Berv, A. Dornburg, et al. 2015. "A Comprehensive Phylogeny of Birds (Aves) Using Targeted Next-Generation DNA Sequencing." *Nature* 526, no. 7574: 569–573. https://doi.org/10.1038/nature15697.

Puelles, L., M. Martínez de la Torre, S. Martinez, C. Watson, and G. Paxinos. 2018. *The Chick Brain in Stereotaxic Coordinates and Alternate Stains*. 2nd ed. Academic Press.

Reiner, A., D. J. Perkel, L. L. Bruce, et al. 2004. "Revised Nomenclature for Avian Telencephalon and Some Related Brainstem Nuclei." *Journal of Comparative Neurology* 473, no. 3: 377–414. https://doi.org/10.1002/CNE.20118.

Rogers, J. H. 1989. "Immunoreactivity for Calretinin and Other Calcium-Binding Proteins in Cerebellum." *Neuroscience* 31, no. 3: 711–721. https://doi.org/10.1016/0306-4522(89)90435-1.

Schindelin, J., I. Arganda-Carreras, E. Frise, et al. 2012. "Fiji: An Open-source Platform for Biological-Image Analysis." *Nature Methods* 9, no. 7: 676–682. https://doi.org/10.1038/NMETH.2019.

Seamans, J. K., and C. R. Yang. 2004. "The Principal Features and Mechanisms of Dopamine Modulation in the Prefrontal Cortex." *Progress in Neurobiology* 74, no. 1: 1–58. https://doi.org/10.1016/j.pneurobio.2004.05.006.

Seed, A., N. Emery, and N. Clayton. 2009. "Intelligence in Corvids and Apes: A Case of Convergent Evolution?" *ethology* 115, no. 5: 401–420. https://doi.org/10.1111/J.1439-0310.2009.01644.X;PAGEGROUP:STRING:PUBLICATION.

Shine, R. 2013. "Reptiles." *Current Biology* 23, no. 6: R227–R231. https://doi.org/10.1016/j.cub.2013.02.024.

Smeets, W. J. A. J., O. Marín, and A. González. 2000. "Evolution of the Basal Ganglia: New Perspectives Through a Comparative Approach." *Journal of Anatomy* 196, no. 4: 501–517. https://doi.org/10.1046/J.1469-7580.2000.19640501.X.

Spool, J. A., M. Macedo-Lima, G. Scarpa, Y. Morohashi, Y. Yazaki-Sugiyama, and L. Remage-Healey. 2021. "Genetically-Identified Neurons in Avian Auditory Pallium Mirror Core Principles of Their Mammalian Counterparts." *Current Biology: CB* 31, no. 13: 2831–2843. https://doi.org/10.1016/J.CUB.2021.04.039.

Stringer, C., T. Wang, M. Michaelos, and M. Pachitariu. 2020. "Cellpose: A Generalist Algorithm for Cellular Segmentation." *Nature Methods* 18, no. 1: 100–106. https://doi.org/10.1038/s41592-020-01018-x.

Unal, G., A. Joshi, T. J. Viney, V. Kis, and P. Somogyi. 2015. "Synaptic Targets of Medial Septal Projections in the Hippocampus and Extrahip-

pocampal Cortices of the Mouse." *Journal of Neuroscience* 35, no. 48: 15812–15826. https://doi.org/10.1523/JNEUROSCI.2639-15.2015.

von Eugen, K., S. Tabrik, O. Güntürkün, and F. Ströckens. 2020. "A Comparative Analysis of the Dopaminergic Innervation of the Executive Caudal Nidopallium in Pigeon, Chicken, Zebra Finch, and Carrion Crow." *Journal of Comparative Neurology* 528, no. 17: 2929–2955. https://doi.org/10.1002/CNE.24878.

Waldmann, C., and O. Güntürkün. 1993. "The Dopaminergic Innervation of the Pigeon Caudolateral Forebrain: Immunocytochemical Evidence for a "Prefrontal Cortex" in Birds?" *Brain Research* 600, no. 2: 225–234. https://doi.org/10.1016/0006-8993(93)91377-5.

Wynne, B., and O. Güntürkün. 1995. "Dopaminergic Innervation of the Telencephalon of the Pigeon (*Columba livia*): A Study With Antibodies Against Tyrosine Hydroxylase and Dopamine." *Journal of Comparative Neurology* 357, no. 3: 446–464. https://doi.org/10.1002/CNE.903570309.

Xiao, L., G. Chattree, F. G. Oscos, M. Cao, M. J. Wanat, and T. F. Roberts. 2018. "A Basal Ganglia Circuit Sufficient to Guide Birdsong Learning." *Neuron* 98, no. 1: 208–221. https://doi.org/10.1016/j.neuron.2018.02.020.

Zahola, P., J. Hanics, A. Pintér, et al. 2019. "Secretagogin Expression in the Vertebrate Brainstem With Focus on the Noradrenergic System and Implications for Alzheimer's Disease." *Brain Structure and Function* 224, no. 6: 2061–2078. https://doi.org/10.1007/S00429-019-01886-W/TABLES/2.

Zaremba, B., A. Fallahshahroudi, C. Schneider, et al. 2025. "Developmental Origins and Evolution of Pallial Cell Types and Structures in Birds." *Science* 387, no. 6735: eadp5182. https://doi.org/10.1126/SCIENCE.ADP5182/SUPPL_FILE/SCIENCE.ADP5182_DATA_S1_TO_S4.ZIP.

Zhao, C., B. Eisinger, and S. C. Gammie. 2013. "Characterization of GABAergic Neurons in the Mouse Lateral Septum: A Double Fluorescence In Situ Hybridization and Immunohistochemical Study Using Tyramide Signal Amplification." *PLoS ONE* 8, no. 8: e73750. https://doi.org/10.1371/JOURNAL.PONE.0073750.